Article

Sodium Percarbonate Activation by Plasma-Generated Ozone for Catalytic Degradation of Dye Wastewater: Role of Active Species and Degradation Process

Jingwen Huang [†], Chendong Puyang [†] and He Guo *

College of Biology and the Environment, Nanjing Forestry University, Nanjing 210037, China; hjw1234560621@163.com (J.H.); pycd182@163.com (C.P.)
* Correspondence: heguo@njfu.edu.cn; Tel.: +86-187-4252-7037
† These authors contributed equally to this work.

Abstract: In this paper, sodium percarbonate (SPC) was activated by ozone (O_3) from plasma for catalytic treatment of dye wastewater. Methyl blue (MB), a typical industrial dye, was selected as the target dye contaminant. Results showed that enhancing O_3 dosage and reducing MB concentration were beneficial to MB degradation. Compared to acid condition, a higher removal efficiency of MB was obtained in alkaline condition. With an increase of SPC dosage, the removal efficiency of MB first was raised, and then it declined. Under the optimal dosage of 50 mg/L, the removal efficiency of MB reached 85.7% with 30 min treatment time. The energy efficiency was improved from 5.21 g/kWh to 5.71 g/kWh. A synergetic effect can be established between O_3 and SPC. Radical capture experiments verified that $\cdot OH$, $\cdot O_2^-$, $^1O_2$, and $\cdot CO_3^-$ played important parts in MB degradation. With increasing reaction time, the amount of total organic carbon (TOC) declined and the amount of ammonia nitrogen (NH_3-N) increased. The addition of SPC enhanced the solution's pH value and conductivity. The degradation pathway was proposed based on density functional theory (DFT) analysis and relevant literatures. The toxicity of MB was alleviated after O_3/SPC treatment. The O_3/SPC process was also suitable for the treatment of other dyes and actual wastewater.

Keywords: sodium percarbonate; ozone; MB; hydrogen peroxide; active species

1. Introduction

The amount of hazardous substances has increased dramatically with the development of industrialization. According to statistics, 10–15% of all dyes are released into the environment during production and use [1]. A great majority of these dyes are very stable and do not easily degrade naturally after entering environmental waters. This can affect the normal life activities of plants and aquatic animals, and even disturb the ecological balance of water bodies [2]. More seriously, dyes are mostly comprised of toxic substances with carcinogenic and teratogenic effects, and their discharge into the environment constitutes a great threat to the health of humans [3]. Therefore, treatment of dye wastewater using efficient technology has become an urgent task.

Various methods have been adopted for the treatment of dye wastewater, such as adsorption [4,5], membrane separation [6,7], ion exchange [8,9], biological treatment [10,11], and advanced oxidation processes (AOPs) [12–14]. Although activated carbon and other physical adsorbents have good adsorption effects, most adsorbents are not ideal for the adsorption of soluble dyes [15]. They easily adsorb large molecular weight and non-polar dyes, but the cost is expensive, making it difficult to use them for the treatment of concentrated pollutants. Membrane separation technology was considered as a new high efficiency separation, concentration, and purification technology, having the advantages of high separation efficiency, simple process, convenient operation, easy control, and no pollution [16]. However, in practical application, the main disadvantages are high

investment and operation costs, membrane clogging, advanced pretreatment, and regular chemical clean. Ion exchange mainly refers to the exchange of ions between wastewater and adsorbent. Although ion exchange can effectively remove dye, the cost of this method is higher, and the exchange membrane needs backwashing and regeneration [17]. Biological methods have been widely studied for dye wastewater treatment because of their low cost, simple operation, and environmental friendliness [18]. The traditional biological treatment technology has been mature, whereas it is difficult to achieve a satisfactory treatment effect since dye wastewater has the characteristic of high concentration and refractory biodegradation. Moreover, the relatively long treatment times and strict reaction conditions have also restricted their development [10].

Currently, AOPs have been deemed some of the most promising technologies for wastewater treatment, including Fenton [19], cavitation [20], ozonation [21], and photocatalytic oxidation [22]. Among these methods, ozonation is usually considered an eco-friendly and practical process for the elimination of dye contaminants. However, its ability to oxidize some dye molecules or their intermediates is very low, leading to limited mineralization efficiency. Moreover, the formation efficiency of free radicals from ozone was relatively low, especially in the acidic pH range. In recent years, the peroxone process has attracted increasing attention because it effectively improves the efficiency of ozone degradation and the mineralization of pollutants [23–25]. In the presence of H_2O_2, more active free radicals will be generated because of accelerated ozone decomposition, which can significantly accelerate pollutant oxidation. However, the rapid decomposition and explosion of liquid H_2O_2 in the process of transportation and storage will bring safety risks. Special facilities are required and relevant practitioners need to be trained before dealing with liquid H_2O_2, which leads to additional costs and limits the practical application [26]. Therefore, the search for alternative oxidants to replace the role of hydrogen peroxide in pollutant remediation has aroused great interest. As a promising in situ chemical oxidation oxidant, sodium percarbonate ($2Na_2CO_3 \cdot 3H_2O_2$, SP), is considered a potential alternative to H_2O_2, and has a wider application prospect in contaminated water since its operation is safer and does not introduce any additional, potentially harmful, byproducts into the water matrix [27–30].

O_3 can be generated via various methods, such as the electrochemical method, the photochemical method, and the dielectric barrier discharge (DBD) plasma method [31]. Of those methods, the DBD plasma method is the most widely used to produce O_3 with lower energy consumption, a larger ozone output per unit, and higher market share [32]. Thus, we proposed the use of SP activated by plasma-generated O_3 for dye wastewater treatment. Methyl blue (MB), a typical industrial dye, can cause adverse symptoms, physiological reactions, and even physiological toxicity with excessive exposure to the environment. Therefore, MP was selected as the target contaminant [33]. The effects of ozone dosage, initial solution concentration, pH value, and SP dosage on dye removal were investigated first. Then, the role of the active species was inspected with various scavengers, including *p*-benzoquinone, isopropanol, triethylenediamine, and indole. Subsequently, the variation of pH, conductivity, total organic carbon (TOC), chemical oxygen demand (COD), and ammonia nitrogen was measured. The degradation pathways were proposed according to density functional theory (DFT) and previous literature. The toxicities of intermediates were estimated based on the US Environmental Protection Agency Toxicity Estimation Software Tool (US-EPA-TEST). Lastly, the application of O_3/SP for other dye degradation and actual wastewater treatment was evaluated.

2. Results

2.1. Effect of O_3 Concentration

O_3 concentration is a critical parameter for the ozonation degradation process. The effect of O_3 concentration on SMX removal was inspected first, and the results are shown in Figure 1a. MB concentration decreased quickly with increasing O_3 concentration, suggesting that higher O_3 concentration was conductive to MB elimination. When concentration

enhanced from 2.0 mg/min to 8.0 mg/min, the removal efficiency increased from 55.9% to 81.7%. The kinetic fitting curve is shown as inset Figure 1a, exhibiting that MB degradation was expedited with higher O_3 concentration. When O_3 concentration was 2.0 mg/min, 4.0 mg/min, 6.0 mg/min, and 8.0 mg/min, the kinetic constant reached 0.030 min^{-1}, 0.049 min^{-1}, 0.055 min^{-1} and 0.067 min^{-1}, respectively. Based on Henry's law, increasing unit volume concentration could increase mass transfer driving force, thus improving O_3 mass transfer rate from gas phase to liquid phase [34]. As a result, the removal efficiency of MB was enhanced with higher O_3 concentration.
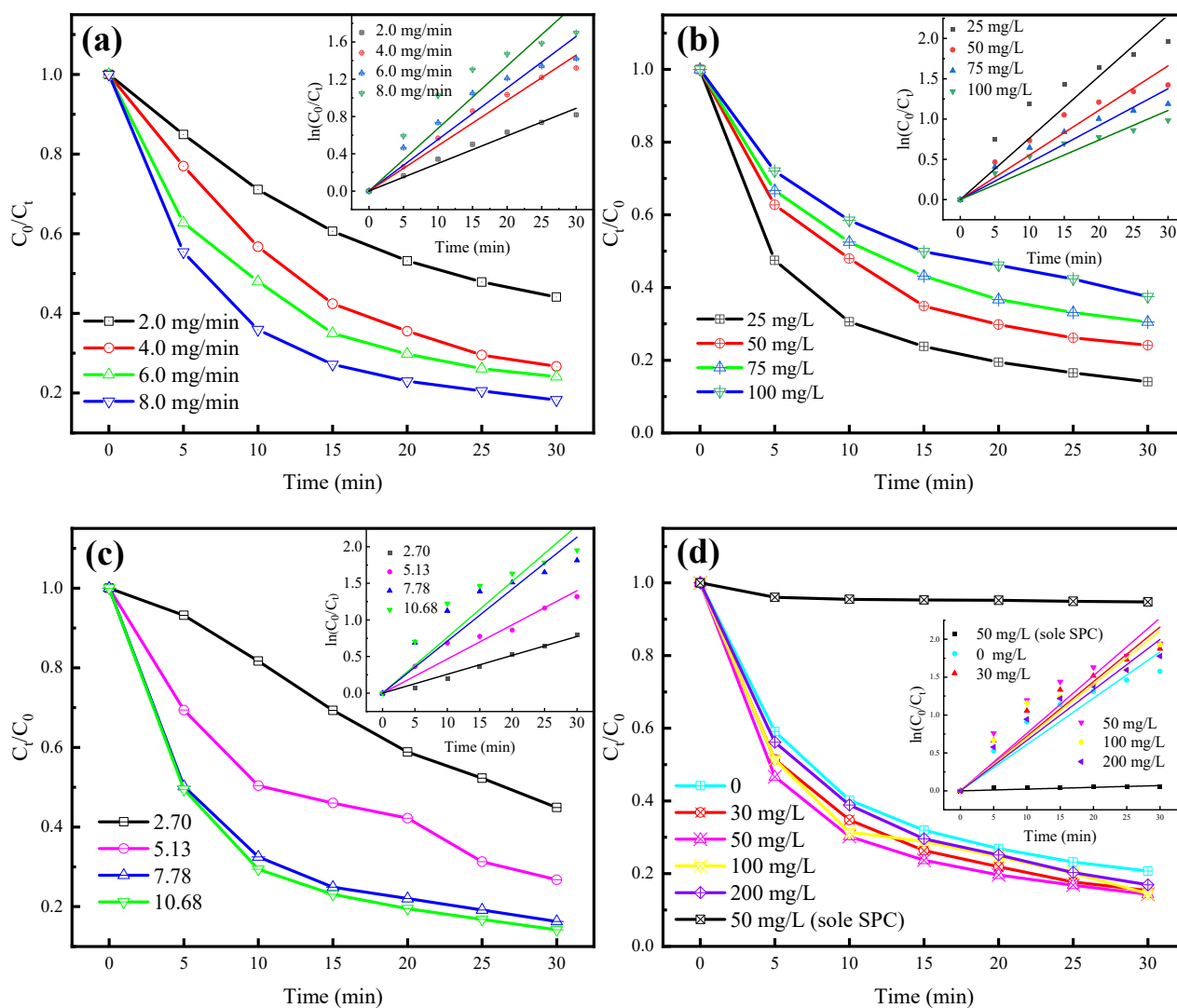
Figure 1. Effect of (**a**) ozone dosage; MB concentration: 25 mg/L, pH value: 7.78, SPC dosage: 50 mg/L (**b**) MB concentration; ozone dosage: 8.0 mg/min, pH value: 7.78, SPC dosage: 50 mg/L (**c**) pH value; ozone dosage: 8.0 mg/min, MB concentration: 25 mg/L, SPC dosage: 50 mg/L (**d**) SPC dosage; ozone dosage: 8.0 mg/min, MB concentration: 25 mg/L, pH value: 7.78.

2.2. Effect of MB Concentration

The removal efficiency of various MB concentrations was shown in Figure 1b. It can be seen that higher MB concentration inhibits MB degradation. When the MB concentration was enhanced from 25 mg/L to 50 mg/L, 75 mg/L, and 100 mg/L, the removal efficiency declined from 85.9% to 75.9%, 69.5%, and 62.6%, respectively. Additionally, the removed quantity of MB increased with higher MB concentration, which reached 21.5 mg, 37.9 mg, 52.1 mg and 62.5 mg under MB concentration of 25 mg/L to 50 mg/L, 75 mg/L, and 100 mg/L, respectively. The inset Figure 1b presents the kinetic fitting curve under various

MB concentrations, illustrating that the MB degradation rate was reduced by higher MB concentration. Under fixed ozone concentration, the produced active species in water was also definite. With an increase of MB concentration, the amount of pollutants and intermediates in the reaction system would be elevated, and a competitive relationship between MB molecules and their degradation intermediates would exist. However, by increasing the initial concentration, the collision probability between MB and active species was raised. Thus, the absolute removal quality of MB was improved. Therefore, the removal efficiency was reduced, but the absolute removal quality was enhanced with increasing MB concentration.

2.3. Effect of pH Value

The pH value is a crucial parameter for wastewater treatment by ozonation, which affects the existence of active substances in water. Figure 1c depicts the effect of solution pH in the range 2.70–10.68 on MB elimination. With an enhancement of pH value, MB elimination was accelerated, which indicated that the alkaline condition was conductive to MB elimination. The removal efficiency improved from 55.1% to 85.8% when pH value increased from 2.70 to 10.68, and the corresponding kinetic constant increased from 0.026 min^{-1} to 0.076 min^{-1} (Figure 1c). As for ozonation, it is widely recognized that direct ozone oxidation is the main process in the acid condition. As for dye decolorization, O_3 could attack the chromophoric group (-N=N-) of dye selectively. Under the alkaline condition, O_3 could be transformed into $\cdot$OH, which possesses a higher oxidation potential and a nonselective characteristic. It can open the ring structure of aromatic dyes, which is beneficial to MB elimination [35]. Thus, a better degradation performance was achieved in the alkaline condition.

2.4. Effect of SP Dosage

The effect of SP dosage on MB elimination is exhibited in Figure 1d. There was almost no removal efficiency for MB elimination with sole SP. Compared to the sole O_3 system, SP addition was conductive to MB degradation. With enhanced SP dosage, the removal efficiency of MB improved at first, and then decreased. The optimal SP dosage was verified as 50 mg/L. Under this condition, the removal efficiency of MB was raised from 79.3% to 85.7% with 30 min treatment time. The corresponding kinetic constants were improved from 0.061 min^{-1} to 0.076 min^{-1} (Figure 1d), respectively. SP could release H_2O_2 in an aqueous solution (Equation (1)).

$$2Na_2CO_3 \cdot 3H_2O_2 \rightarrow 2Na_2CO_3 + 3H_2O_2 \tag{1}$$
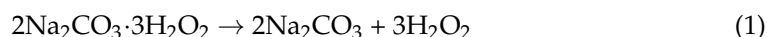
In the O_3 system, when SP was added, the released H_2O_2 reacted with O_3 and generated a peroxygenation reaction, which accelerated the formation of $\cdot$OH [36]. In addition, an alkaline solution environment could be generated when SP was added in the O_3 system. It is well known that O_3 was conductive to transform into $\cdot$OH (Equations (2)–(7)), which could also promote MB elimination.

$$O_3 + H_2O_2 \rightarrow 2 \cdot OH + 3O_2 \tag{2}$$

$$O_3 + OH^- \rightarrow HO_2^- + O_2 \tag{3}$$

$$O_3 + HO_2^- \rightarrow \cdot HO_2 + O_3^- \tag{4}$$

$$\cdot HO_2^- \leftrightarrow \cdot O_2^- + H^+ \tag{5}$$

$$\cdot O_3^- + H^+ \rightarrow \cdot HO_3 \tag{6}$$

$$\cdot HO_3 \rightarrow \cdot OH + O_2 \tag{7}$$

However, excess SP in O_3 system would block the interaction between the MB molecule and the active substance. On the other side, excess SP would release a large amount of

H_2O_2, and it would react with $\cdot OH$ and consume $\cdot OH$ (Equations (8)–(12)) [37]. As a result, excess SP dosage hindered MB degradation in the O_3 system.

$$H_2O_2 \rightarrow O_2 + H_2O \tag{8}$$

$$H_2O_2 + \cdot OH \rightarrow \cdot HO_2^- + H_2O \tag{9}$$

$$HO_2^- + \cdot OH \rightarrow \cdot HO_2^- + OH^- \tag{10}$$

$$HCO_3^- + \cdot OH \rightarrow \cdot CO_3^- + H_2O \tag{11}$$

$$CO_3^{2-} + \cdot OH \rightarrow \cdot CO_3^- + OH^- \tag{12}$$
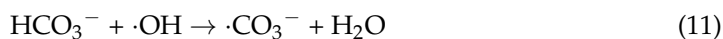
Economic benefit is a significant index for evaluating a technology, and therefore energy efficiency under various SP dosages were calculated (Table 1). It was noted that the energy efficiency in the O_3/SP system was higher than that in the sole O_3 system. When SP dosage was 50 mg/L, the energy efficiency reached 5.71 g/kWh with 30 min treatment time, which was higher than that (5.29 g/kWh) in the sole O_3 system. It was summarized that SP addition could lead to energy conservation for practical application. Synergy factor was adopted to assess the synergy efficiency between various systems [37]. Table 1 also exhibits a synergy effect between O_3 and SP. It can be seen that the highest synergy factor was obtained when SP dosage was selected as 50 mg/L, which could reach 1.20. Furthermore, it was worth noting that all synergy factors were greater than 1, demonstrating that a synergy effect could be formed between O_3 and SP.

Table 1. Energy efficiency and synergetic factor.

SPC Addition (mg/L)	Energy Efficiency (g/kWh)						Synergetic Factor
	5 min	10 min	15 min	20 min	25 min	30 min	
0	16.36	11.95	9.07	7.31	6.15	5.29	——
30	17.53	12.22	9.39	7.40	6.38	5.54	1.14
50	21.33	13.95	10.17	8.04	6.66	5.71	1.20
100	19.43	13.72	9.48	7.53	6.39	5.70	1.11
200	19.43	13.04	9.82	7.81	6.58	5.65	1.05

2.5. Role of Active Species

For the free radical capture experiment, different concentrations of free radicals were added to the reaction solution, the effect of different concentrations of free radicals on the degradation efficiency was investigated, and the role of free radicals was given. The potential reactive oxygen species generated in the O_3/SP system were evaluated using various radical scavengers. Based on the peroxidation theory, $\cdot OH$ formation could be promoted by O_3 and H_2O_2, thereby accelerating pollutant degradation. Therefore, isopropanol was selected to distinguish the role of $\cdot OH$ due to the extreme reaction rate (10^9 M^{-1} S^{-1}) between isopropanol and $\cdot OH$ [38]. The rate is higher than that of isopropanol and other radicals. The corresponding results are shown in Figure 2. It can be seen that MB degradation was greatly inhibited by the addition of isopropanol (Figure 2a). The removal efficiency of MB clearly declined with a higher concentration of isopropanol, declining from 88.5% to 66.0% with 1.00 mmol/L isopropanol (Figure 2b). The result indicated the involvement of $\cdot OH$ in the degradation of MB.
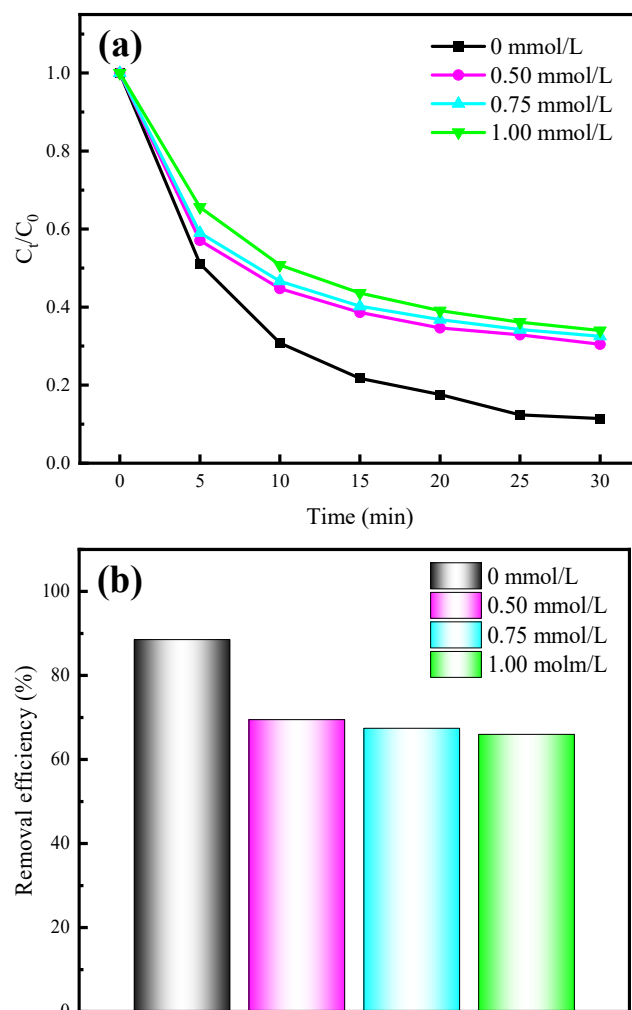
Figure 2. Effect of isopropanol: (**a**) degradation curve; (**b**) removal efficiency with 30 min treatment. Ozone dosage: 8.0 mg/min, other experimental condition was consistence with Figure 1a.

It has been reported that liquid O_3 could transform into $\cdot O_2^-$, which possesses higher oxidation capacity, allowing it to participate in contaminant decomposition [39]. Herein, a typical $\cdot O_2^-$ scavenger, *p*-benzoquinone was adopted to inspect the role of $\cdot O_2^-$, and the result is shown in Figure 3. It can be seen that, after *p*-benzoquinone addition, MB removal efficiency was diminished, and the inhibition was strengthened by enhancing the *p*-benzoquinone concentration (Figure 3a). The removal efficiency was significantly reduced from 88.5% to 30.2% with 3 mmol/L *p*-benzoquinone (Figure 3b), suggesting that $\cdot O_2^-$ was definitely involved in the destruction of MB.

Recent literature has shown that $^1O_2$ with higher oxidation potential could decompose organic compounds through electrophilic reactions [40]. In the O_3/SP system, $\cdot OH$ could react with $\cdot O_2^-$ and lead to the generation of $^1O_2$ (Equations (13)–(15)). Therefore, in order to clarify the role of $^1O_2$, triethylenediamine was chosen as the $^1O_2$ scavenger. The effect of triethylenediamine addition on MB elimination is depicted in Figure 4. MB degradation was significantly impeded in the presence of triethylenediamine (Figure 4a). When the concentration of triethylenediamine was 1 mmol/L, 2 mmol/L, or 3 mmol/L, the removal efficiency of MB declined from 88.5% to 46.5%, 37.5%, and 30.2%, respectively (Figure 4b). Therefore, it can be confirmed that $^1O_2$ acted as a critical radical responsible for MB degradation.

$$\cdot O_2^- + \cdot OH \rightarrow {}^1O_2 + OH^- \tag{13}$$

$$\cdot O_2^- + \cdot HO_2 + H^+ \rightarrow {}^1O_2 + H_2O_2 \tag{14}$$

$$\cdot HO_2 + \cdot HO_2 \rightarrow {}^1O_2 + H_2O_2 \tag{15}$$
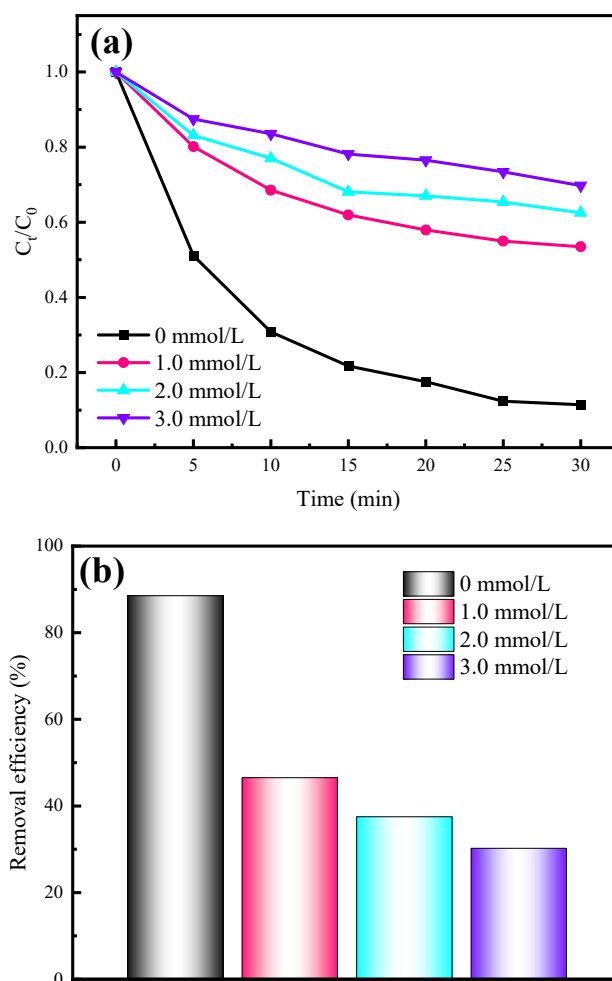
Figure 3. Effect of *p*-benzoquinone: (**a**) degradation curve; (**b**) removal efficiency with 30 min treatment. Ozone dosage: 8.0 mg/min, other experimental condition was consistence with Figure 1a.

Na$_2$CO$_3$ and H$_2$O$_2$ could be released when SP was added in water. The generated CO$_3^{2-}$ could react with ·OH, or HCO$_4^-$ could self-decompose and form ·CO$_3^-$ (Equations (16) and (17)) [29], which could contribute to organic contaminant degradation. To inspect the role of ·CO$_3^-$, we conducted the experiment with indole (10^6 M^{-1} S^{-1}) present, a known quencher of ·CO$_3^-$ [41]. The result is given in Figure 5. The addition of indole evidently decreased the removal efficiency of MB (Figure 5a). Approximately 88.6% removal efficiency could be achieved after 30 min treatment time without indole, which declined to 56.0% with 5.0 mmol/L indole (Figure 5b). These results suggested that ·CO$_3^-$ might account for MB degradation in O$_3$/SP systems.

$$CO_3^{2-} + \cdot OH \rightarrow \cdot CO_3^- + OH^- \tag{16}$$

$$HCO_4^- \rightarrow \cdot CO_3^- + OH \tag{17}$$
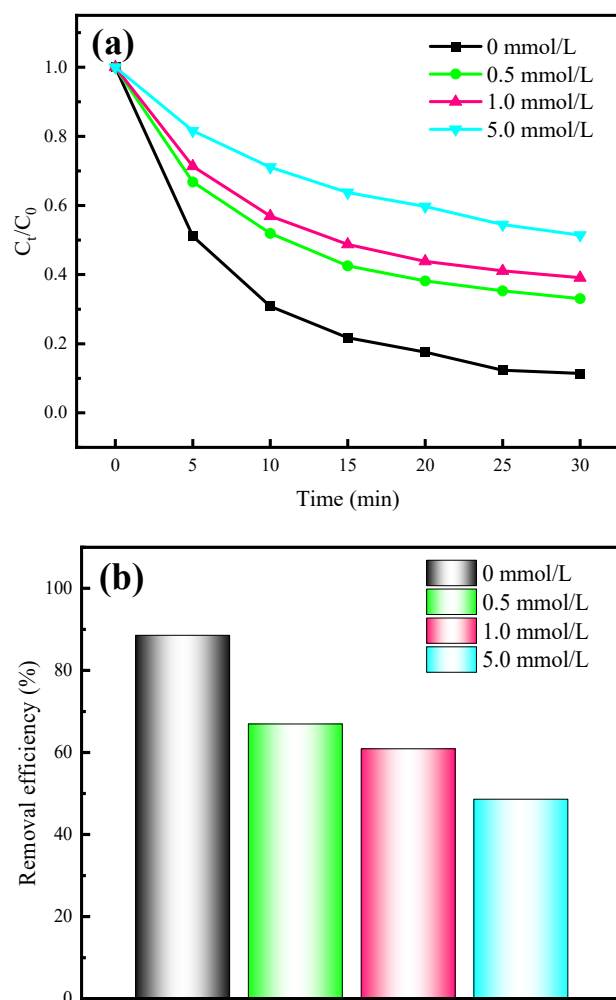
Figure 4. Effect of triethylenediamine: (**a**) degradation curve; (**b**) removal efficiency with 30 min treatment. Ozone dosage: 8.0 mg/min, other experimental condition was consistence with Figure 1a.

2.6. UV-Vis Spectra, TOC Removal and Fluorescence Excitation-Emission Matrix Spectra

MB degradation processes at different regular time intervals were estimated by UV-Vis absorption spectra, as shown in Figure 6a. The main peak was located at 309 nm, with a gradual decrease in absorption intensity with an increase in reaction time. These phenomena suggested that MB molecules were decomposed efficiently. Additionally, it is worth noting that the intensity located at the period from 222–268 nm raised as time went on, compared to the original intensity, illustrating that degradation intermediates could be generated. In addition, in the process of degradation, a decolorization of the MB solution occurred, changing from dark blue to light blue to colorless, which meant that the concentration of MB decreased. Figure 6b presents the TOC value under various reaction times. With prolonging treatment time, TOC value was dropped. After 30 min treatment time, TOC value was reduced from 6.3 mg/L to 5.1 mg/L, indicating that MB molecules can be mineralized by O_3/SP, although many degradation intermediates were produced.

Fluorescence excitation-emission matrix spectroscopy was evaluated to investigate the decay of MB [42]. Figure 7a exhibits the spectra in the range of emission wavelength 350–600 nm and excitation wavelength 250–600 nm, the fluorescence peaks corresponded to the profile of a humic acid-like substance, suggesting that the structure of MB molecules was similar to that of humic acid [42]. With increasing the reaction time, the peak intensity declined, illustrating that the humic acid-like molecular structure can be destroyed (Figure 7b,c). After 30 min treatment, the fluorescence peaks shifted, possibly due to the interference of degradation intermediates (Figure 7d). An analogous phenomenon was

also observed by Zhu, et al. [43]. Therefore, it can be concluded that MB molecules can be successfully decomposed by the O_3/SP process.
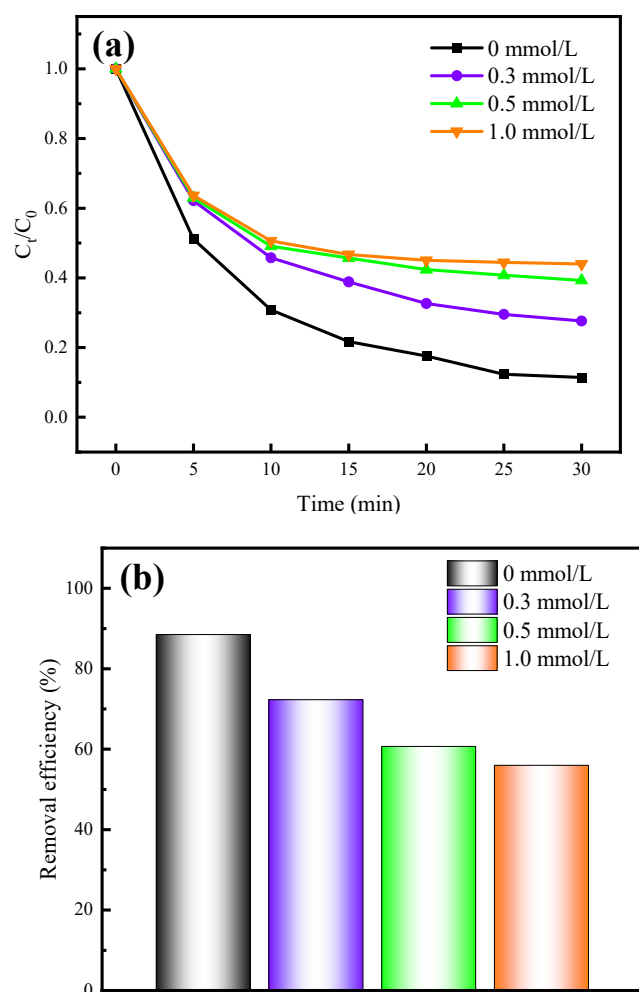
Figure 5. Effect of indole: (**a**) degradation curve; (**b**) removal efficiency with 30 min treatment. Ozone dosage: 8.0 mg/min, other experimental condition was consistence with Figure 1a.

2.7. Variation of pH, Conductivity, and Ammonia Nitrogen

The changes in pH and conductivity under variation reaction systems were shown in Figure 8. Compared to the O_3 system, the O_3/SP system obtained a higher pH value. Meanwhile, the conductivity of the MB solution was enhanced after SP addition. These results are attributed to the released CO_3^{2-} and Na^{2+} in the MB solution, which could enhance the pH value and the conductivity. With increasing treatment time, the pH value decreased. After treatment for 30 min, the pH value declined from a range of 9.64 to 6.81 in the O_3/SP system. This was attributed to the generation of organic acid and inorganic acid during MB degradation [44]. Additionally, the conductivity was increased from 93.2 μS/cm to 144.8 μS/cm in the O_3/SP system after treatment for 30 min. During MB degradation, NH_4^+, SO_4^{2-}, and Na^+ can be produced, which would enhance conductivity. From Figure 9, it was found that the amount of NH_3-N increased with the delay of processing time, which may be because the nitrogen atom that exists in MB molecules could be mineralized into the free form of NH_3-N.
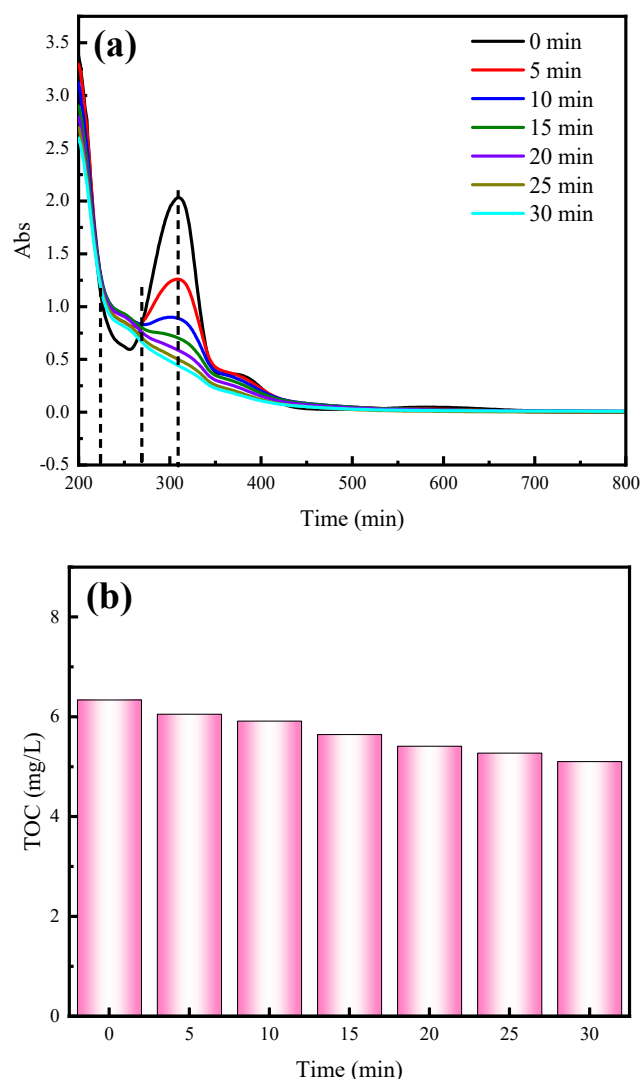
Figure 6. (**a**) UV-Vis spectra of MB and (**b**) TOC under various treatment time.

2.8. Degradation Pathway

To explore the degradation pathway of MB, a DFT analysis with the CASTEP module and the Dmol 3 module was performed, illustrating the f^0, population, and length of MB molecules. It is worth mentioning that the MB molecule was divided into three major modules, and two of the major modules were similar. The two major module divisions are shown in Tables 2 and 3. Based on calculated results and literature, we proposed the MB degradation pathway, which is shown in Figure 10. Firstly, the MB central aromatic ring was broken and then the side aromatic rings were ruptured, which produced P1 and P4 [45]. Then C=C was attacked by free radicals, leading to the transformation from P1 to P2. Table 2 shows that S (15) possesses relative large f^0. Table 3 shows that C13–S1 have relatively small populations and large lengths. Therefore, P2 was converted into P3. Then, unstable C=N was attacked by free radicals, which induced the P3 change to P5. On the other hand, a conversion from P4 into P5 occurred, similar to the conversion from P2 to P3. Then, the N atom of P5 was apt to attack, resulting in the formation of P6. Then, the ring-opening reaction process of the intermediates occured, which further converted these intermediates to CO_2, H_2O, SO_4^{2-}, NH_4^+, Na^+, and the final oxidation products [46,47].
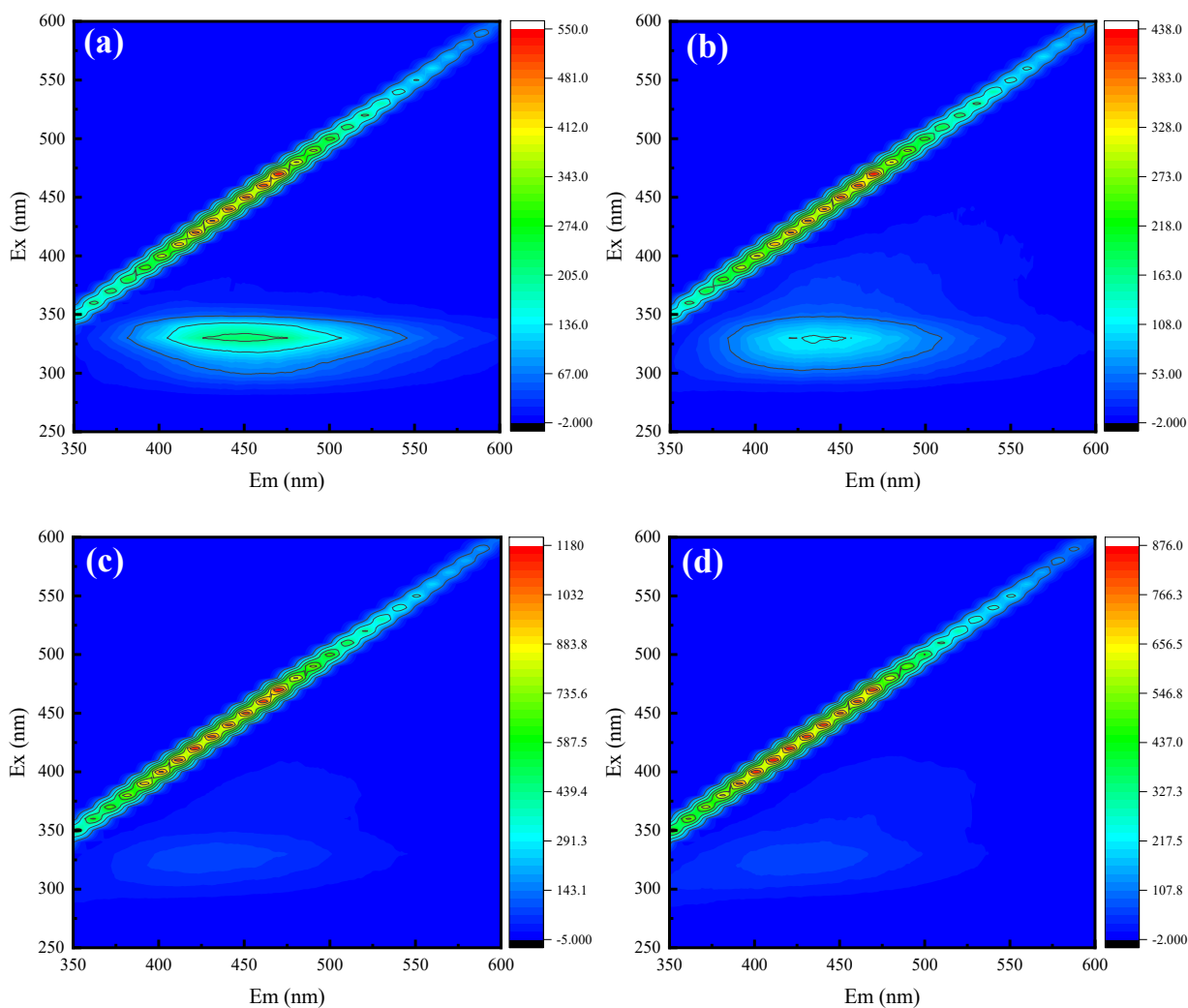
Figure 7. Fluorescence excitation-emission matrix spectra of MB with various reaction time: (**a**) 0 min; (**b**) 10 min; (**c**) 20 min; (**d**) 30 min.
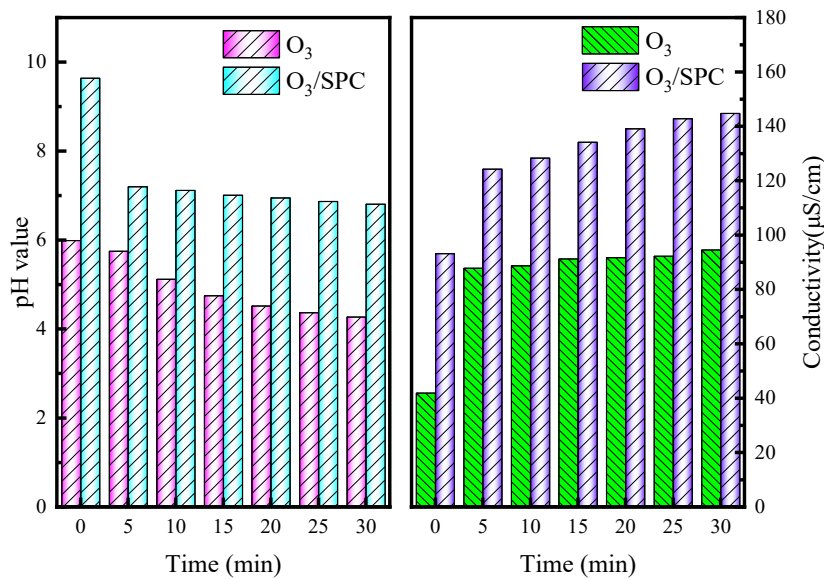
Figure 8. Variation of pH and conductivity under various treatment time.
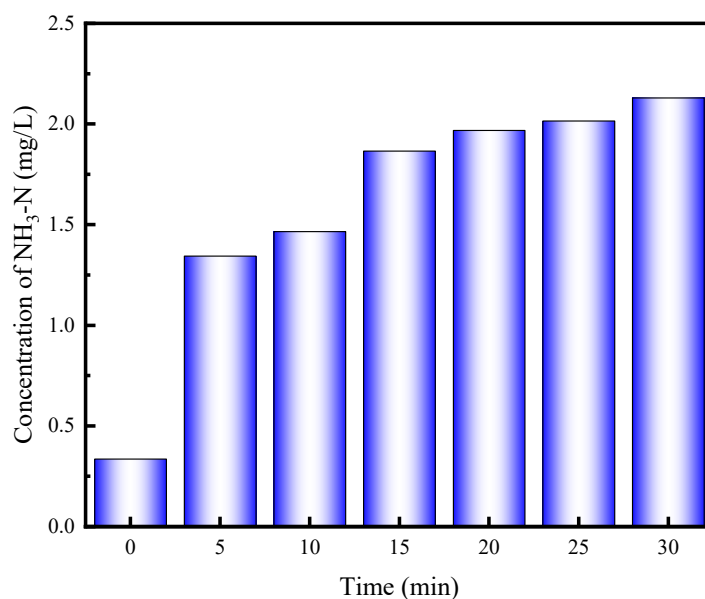
Figure 9. Variation of NH$_3$-N under various treatment time.

Table 2. DFT analysis results of MB molecule with DMol3 module.

Molecular Formula and Atomic Number	Atom	f^0	Atom	f^0	Atom	f^0
	C(1)	0.028	C(11)	0.016	H(21)	0.041
	C(2)	−0.009	C(12)	0.024	H(22)	0.032
	C(3)	0.018	C(13)	0.012	H(23)	0.052
	C(4)	0.025	C(14)	0.002	H(24)	0.051
	C(5)	0.022	S(15)	0.060	H(25)	0.043
	C(6)	0.016	O(16)	0.077	H(26)	0.013
	C(7)	0.085	O(17)	0.084	H(27)	0.045
	N(8)	0.022	O(18)	0.058	H(28)	0.029
	C(9)	0.020	H(19)	0.042	H(29)	0.054
	C(10)	0.024	H(20)	0.015		

Table 3. DFT analysis results of MB molecule with CASTEP module.

	Bond	Population	Length (A)	Bond	Population	Length (A)
	H2-H8	−0.20	0.73	C11-C12	1.00	1.54
	H11-O3	0.45	1.11	C2-C4	0.93	1.54
	H7-C9	0.82	1.14	C4-C6	1.08	1.54
	H10-C12	0.82	1.14	C8-C10	0.99	1.54
	H5-C7	0.79	1.14	C5-C6	0.93	1.54
	H9-C11	0.82	1.14	C9-C10	1.04	1.54
	H4-C6	0.80	1.14	C1-C3	1.08	1.54
	H6-C7	0.79	1.14	C2-C7	0.99	1.54
	H1-C1	0.82	1.14	C1-C2	0.93	1.54
	H8-C10	1.10	1.14	C12-C13	0.99	1.54
	H3-C4	0.83	1.14	C8-C13	0.95	1.54
	H2-C3	1.09	1.14	O2-S1	0.43	1.78
	C5-N1	0.85	1.50	O3-S1	0.18	1.78
	C8-N1	0.81	1.51	O1-S1	0.44	1.78
	C3-C5	0.93	1.54	C13-S1	0.54	1.81
	C9-C11	0.96	1.54			
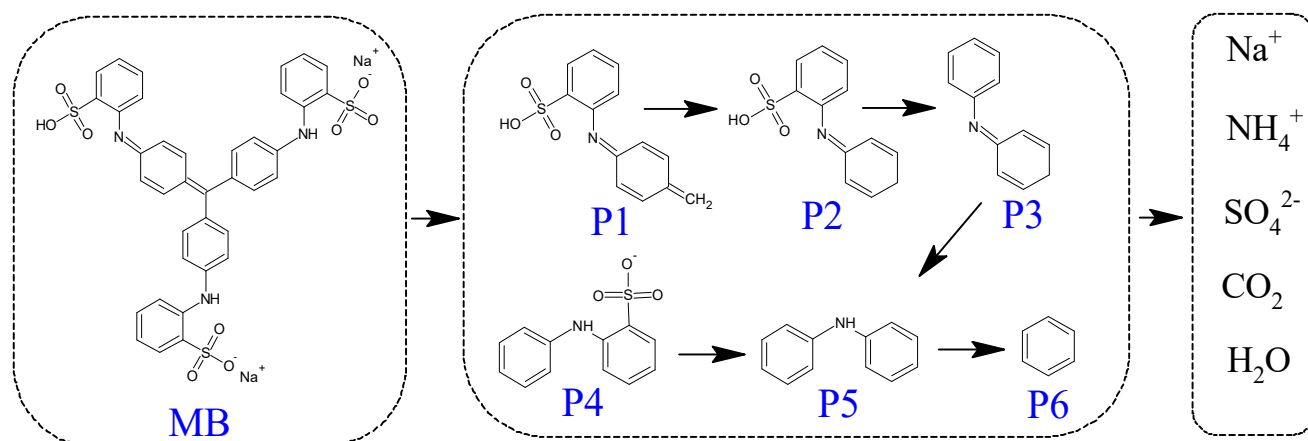
Figure 10. Degradation pathway of MB with O_3/SPC treatment.

2.9. Toxicity Evaluation

To further understand the toxicity of intermediates, a toxicity assessment of MB and its intermediates was performed using a quantitative structure–activity relationship (QSAR) program based on the QSAR method. In this process, evaluation indexes including oral rat LD_{50}, developmental toxicity, and mutagenicity were chosen. As shown in Figure 11a, aside from P3, the LD_{50} content of all intermediates were located in the "Toxic" or "Very toxic" regions. It is worth noting that the LD_{50} content of P4 cannot be predicted due to a limited database. Figure 11b depicts the developmental toxicity of MB and degradation intermediates. It can be noted that P1–P4 were situated at "developmental toxicant", while P5 and P6 were situated at "developmental non-toxicant". Figure 11c exhibits the mutagenicity of MB as "Mutagenicity positive". Surprisingly, the mutagenicities of all intermediates were situated in the "Mutagenicity negative" range. By comprehensive analysis of toxicity evaluation results, it can be summarized that the toxicity of MB could be relieved after O_3/SP treatment.

2.10. For Other Dye Removal and Actual Wastewater Treatment

In order to figure out the feasibility of the technology for the degradation of other dyes, congo red, methyl orange, and rhodamine B were selected. Figure 12a shows that the removal efficiency of all dyes was higher than 90% after 30 min treatment time. Furthermore, the kinetic constant also exhibited a higher value. These results indicated that the current process was also suitable for the treatment of dye wastewater. In order to figure out the O_3/SP process for actual wastewater treatment, we selected underground wastewater from our university. Figure 12b illustrated that COD value decreased with an increase in reaction time. After 30 min treatment, COD declined from 243.3 mg/L to 205.7 mg/L. Therefore, it can be summarized that the O_3/SP process for actual wastewater treatment is feasible by further increasing the treatment time.
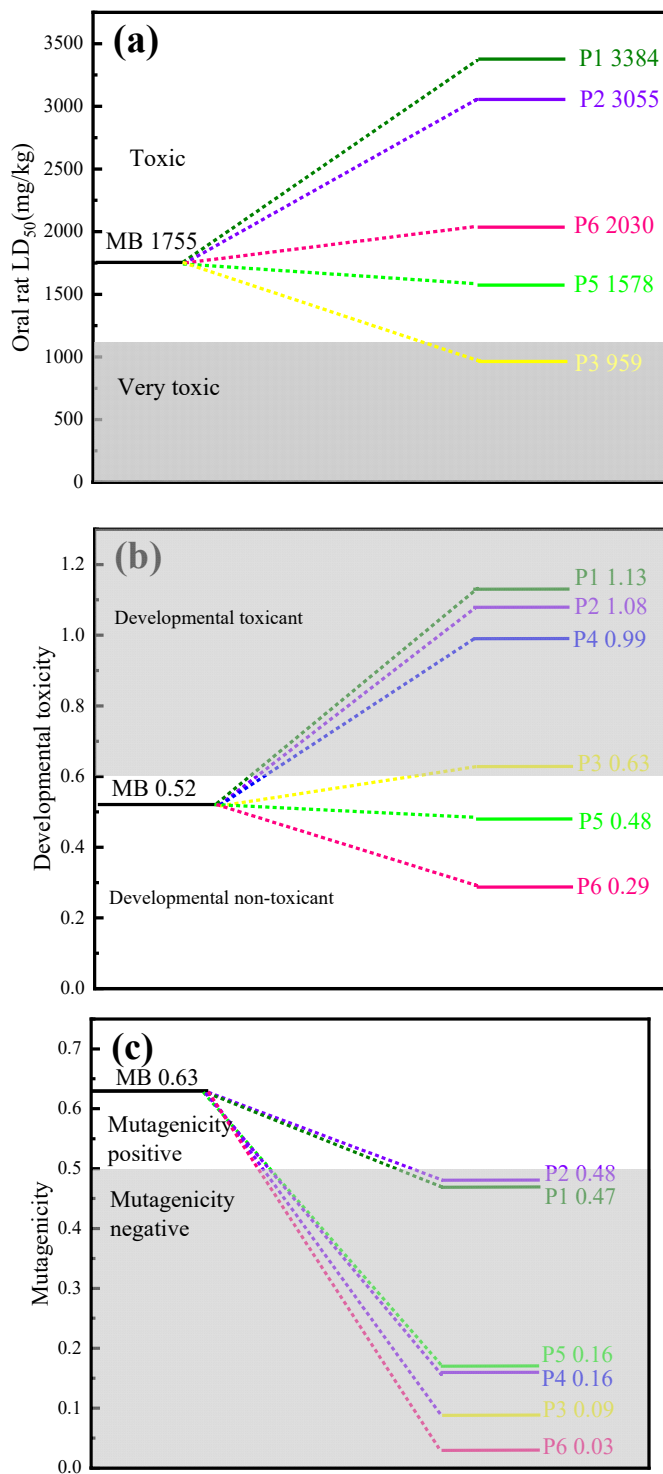
Figure 11. Toxicity assessment: (**a**) Oral rat LD50; (**b**) Developmental toxicity; (**c**) Mutagenicity.
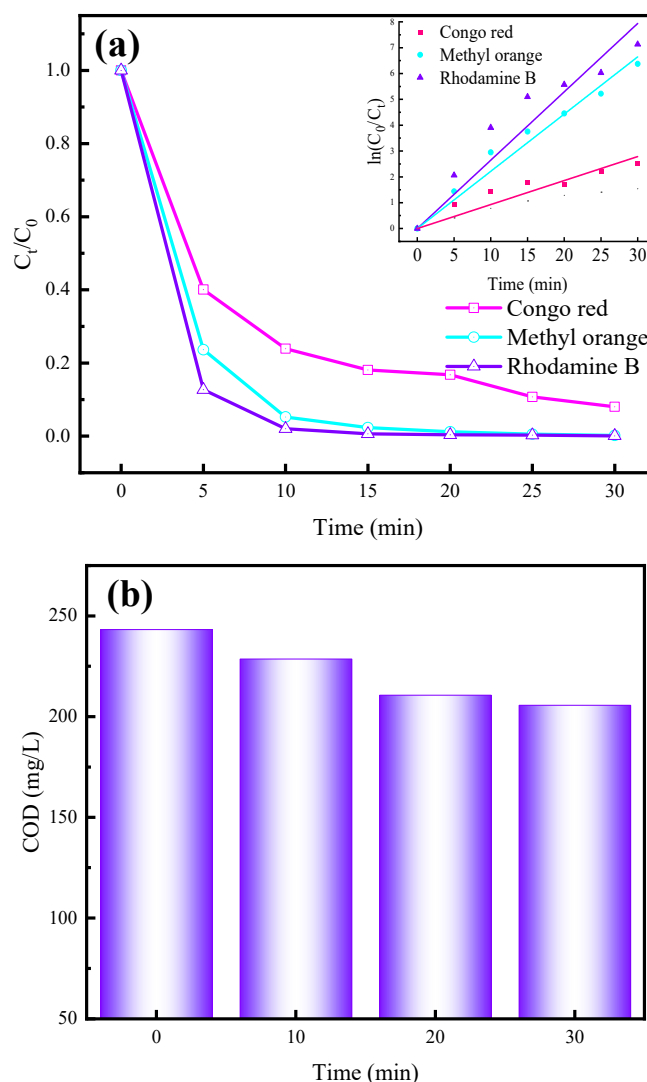
Figure 12. (**a**) Applied for other dyes degradation; (**b**) COD removal for actual wastewater.

3. Materials and Methods

3.1. Chemicals

MB, SP, terephthalic acid, sodium hydroxide, and sodium indigo disulfonate (IDS) were obtained from Aladdin Reagent Co., Ltd. (Shanghai, China) Titanium oxysulfate, hydrogen peroxide 30% aqueous solution, isopropanol (IPA), *p*-benzoquinone, phosphoric acid, and indole were bought from Sinopharm Chemical Reagent Co., Ltd. (Beijing, China) All aqueous solution was prepared with deionized water, which was prepared by high purity water machine (Biosafer-10R, East Hartford, CT, USA).

3.2. Degradation Analysis

O_3 was formed by a DBD plasma ozone generator (Changqing, CQ-802S, Nanjing, China). The reactor was as a cylindrical form style, and the diameter and height were 8 cm and 15 cm, respectively. The concentration was regulated by an atmospheric sampling instrument (Laobao, QC-350, Qingdao, China). Concentration of MB was detected by UV-Vis spectrograph (METASH, UV-5500PC, Shanghai, China) with a detection wavelength of 311 nm. The sampled time was set as every 5 min. The degradation efficiency was calculated as follows:

$$\eta = \frac{C_0 - C_t}{C_0} \tag{18}$$

where C_0 is the initial concentration of MB, mg/L; C_t is concentration of MB under t time; mg/L. The degradation kinetic was calculated according to pseudo-first order dynamic model, which is shown as follows [47]:

$$\ln(\frac{C_0}{C_t}) = kt \tag{19}$$

where C_0 and C_t are defined as the same mean-like formula (18); k is the kinetic constant, $\min^{-1}$; t is the sample time, min. The energy efficiency was calculated as follows [48]:

$$E = \frac{(\eta \times C_0)}{Pt} \tag{20}$$

where C_0, η and t are defined as the same mean-like formula (18); P is the power of the plasma generator.

The synergistic effect between O_3 and SP was calculated on the basis of the kinetic constant, shown as:

$$SF = \frac{k_{O_3+SP}}{k_{O_3} + k_{SP}} \tag{21}$$

where SF is the synergistic factor; k_{O_3+SP} is the kinetic constant for O_3/SP; k_{O_3} is the kinetic constant for sole O_3; k_{SP} is the kinetic constant for sole SP. During the experiment, SP was dispersed in MB solution evenly. The conductivity and pH were tested by conductivity meter (INESA, DDS-307A, Shanghai, China) and pH meter (INESA, PHS-3C), respectively. TOC detector (SHMADZU, TOC-V CPN, Kyoto, Japan) was adopted to measure TOC. The water quality detector (Lian hua, 5B-6C, Beijing, China) was utilized to test ammonia nitrogen and COD. The fluorescence characteristic of MB molecules was inspected by fluorescence spectrometer (F97Pro, Lingguang, Shanghai, China).

3.3. DFT Analysis and Toxicity Assays

In order to predict the degradation pathway of MB, f^0, population and length of MB molecules were calculated based on DFT analysis, which was carried out on Material Studio (MS, version 4.2.1) [49]. The equipped CASTEP module was taken to compute the population, giving the result of population and length. During this calculation, a crystal with parameters of $15 \times 15 \times 15$ A was established. The equipped Dmol 3 module was performed to present Fukui Function, giving the result of f^0 [50,51]. The intermediates toxicity was assessed by US Environmental Protection Agency Toxicity Estimation Software Tool (US-EPA-TEST) based on oral rat LD_{50}, developmental toxicity and mutagenicity [52].

4. Conclusions

Herein, SP activated by plasma-generated O_3 for dye wastewater treatment was investigated. The effects of ozone dosage, initial MB concentration, pH value, and SP dosage on MB removal was first investigated. A higher removal efficiency of MB was achieved at a higher ozone dosage, lower MB concentration, and higher pH value. The addition of SP could accelerate MB degradation in an O_3 system. Energy efficiency can be enhanced with SP addition. Active species consisting of $\cdot OH$, $\cdot O_2^-$, $^1O_2$, and $\cdot CO_3^-$ participated in MB degradation. UV-Vis spectra and fluorescence excitation–emission matrix spectra verified that MB molecules could be decomposed successfully. The pH value and conductivity increased after SP addition. The pH value decreased and conductivity increased as treatment time went on. Additionally, the amount of NH_3-N increased with prolonged reaction time. According to DFT analysis and literature, a degradation pathway of MB was proposed, which mainly involved the rupture of the central aromatic ring, C=C, and C=N. Toxicity indexes including oral rat LD_{50}, developmental toxicity, and mutagenicity were assessed. Treatment of other dyes and actual wastewater was feasible by the O_3/SP process.

References

1. Donkadokula, N.Y.; Kola, A.K.; Naz, I.; Saroj, D. A review on advanced physico-chemical and biological textile dye wastewater treatment techniques. *Rev. Environ. Sci. Bio.* **2020**, *19*, 543–560. [CrossRef]
2. Yaseen, D.A.; Scholz, M. Textile dye wastewater characteristics and constituents of synthetic effluents: A critical review. *Int. J. Environ. Sci. Technol.* **2019**, *16*, 1193–1226. [CrossRef]
3. Paździor, K.; Bilińska, L.; Ledakowicz, S. A review of the existing and emerging technologies in the combination of AOPs and biological processes in industrial textile wastewater treatment. *Chem. Eng. J.* **2019**, *376*, 120597. [CrossRef]
4. Chen, R.; Cai, J.; Li, Q.; Wei, X.; Min, H.; Yong, Q. Coadsorption behaviors and mechanisms of Pb (II) and methylene blue onto a biodegradable multi-functional adsorbent with temperature-tunable selectivity. *RSC Adv.* **2020**, *10*, 35636. [CrossRef]
5. Li, W.; Mu, B.; Yang, Y. Feasibility of industrial-scale treatment of dye wastewater via bio-adsorption technology. *Bioresour. Technol.* **2019**, *277*, 157–170. [CrossRef]
6. Yang, Y.; Wang, H.; Li, J.; He, B.; Wang, T.; Liao, S. Novel functionalized nano-TiO$_2$ loading electrocatalytic membrane for oily wastewater treatment. *Environ. Sci. Technol.* **2012**, *46*, 6815–6821. [CrossRef]
7. Damodar, R.A.; You, S.J.; Ou, S.H. Coupling of membrane separation with photocatalytic slurry reactor for advanced dye wastewater treatment. *Sep. Purif. Technol.* **2010**, *76*, 64–71. [CrossRef]
8. Raghu, S.; Basha, C.A. Chemical or electrochemical techniques, followed by ion exchange, for recycle of textile dye wastewater. *J. Hazard. Mater.* **2007**, *149*, 324–330. [CrossRef]
9. Labanda, J.; Sabaté, J.; Llorens, J. Experimental and modeling study of the adsorption of single and binary dye solutions with an ion-exchange membrane adsorber. *Chem. Eng. J.* **2011**, *166*, 536–543. [CrossRef]
10. Khalid, A.; Arshad, M.; Crowley, D.E. Biodegradation potential of pure and mixed bacterial cultures for removal of 4-nitroaniline from textile dye wastewater. *Water Res.* **2009**, *43*, 1110–1116. [CrossRef]
11. Kanagaraj, J.; Senthilvelan, T.; Panda, R.C. Degradation of azo dyes by laccase: Biological method to reduce pollution load in dye wastewater. *Clean Technol. Environ. Policy* **2015**, *17*, 1443–1456. [CrossRef]
12. Arslan-Alaton, I. A review of the effects of dye-assisting chemicals on advanced oxidation of reactive dyes in wastewater. *Color. Technol.* **2003**, *119*, 345–353. [CrossRef]
13. Papi, S.; Koprivanac, N.; Boi, A.L.; Vujevi, D.; Dragievi, S.K.; Peternel, H.K. Advanced oxidation processes in azo dye wastewater treatment. *Water Environ. Res.* **2006**, *78*, 572–579. [CrossRef]
14. Vaiano, V.; Iervolino, G.; Rizzo, L.; Sannino, D. Advanced oxidation processes for the removal of food dyes in wastewater. *Curr. Org. Chem.* **2017**, *21*, 1068–1073. [CrossRef]
15. Mu, B.; Wang, A. Adsorption of dyes onto palygorskite and its composites: A review. *J. Environ. Chem. Eng.* **2016**, *4*, 1274–1294. [CrossRef]
16. Thamaraiselvan, C.; Noel, M. Membrane processes for dye wastewater treatment: Recent progress in fouling control. *Crit. Rev. Environ. Sci. Technol.* **2015**, *45*, 1007–1040. [CrossRef]
17. Joseph, J.; Radhakrishnan, R.C.; Johnson, J.K.; Joy, S.P.; Thomas, J. Ion-exchange mediated removal of cationic dye-stuffs from water using ammonium phosphomolybdate. *Mater. Chem. Phys.* **2019**, *242*, 122488. [CrossRef]
18. Masoudnia, S.; Juybari, M.H.; Mehrabian, R.Z.; Ebadi, M.; Kaveh, F. Efficient dye removal from wastewater by functionalized macromolecule chitosan-sba-15 nanofibers for biological approaches. *Int. J. Biol. Macromol.* **2020**, *165*, 118–130. [CrossRef]
19. Zhang, M.H.; Zhao, D.H.L.; Wang, D.X.; Meng, D. A review on fenton process for organic wastewater treatment based on optimization perspective. *Sci. Total Environ.* **2019**, *670*, 110–121. [CrossRef]
20. Bagal, M.V.; Gogate, P.R. Wastewater treatment using hybrid treatment schemes based on cavitation and Fenton chemistry: A review. *Ultrason. Sonochem.* **2014**, *21*, 1–14. [CrossRef]
21. Jahan, B.N.; Li, L.; Pagilla, K.R. Fate and reduction of bromate formed in advanced water treatment ozonation systems: A critical review. *Chemosphere* **2020**, *266*, 128964. [CrossRef] [PubMed]

22. Chong, M.N.; Jin, B.; Chow, C.W.; Saint, C. Recent developments in photocatalytic water treatment technology: A review. *Water Res.* **2010**, *44*, 2997–3027. [CrossRef]

23. Turkay, O.; Ersoy, Z.G.; Bar, S. Review-the application of an electro-peroxone process in water and wastewater treatment. *J. Electrochem. Soc.* **2017**, *164*, E94–E102. [CrossRef]

24. Chen, H.; Wang, J. Degradation and mineralization of ofloxacin by ozonation and peroxone (O_3/H_2O_2) process. *Chemosphere* **2021**, *269*, 128775. [CrossRef]

25. Li, S.; Huang, J.; Ye, Z.; Wang, Y.; Li, L. The mechanism of metal-H_2O_2 complex immobilized on mcm-48 and enhanced electron transfer for effective peroxone ozonation of sulfamethazine. *Appl. Catal. B-Environ.* **2021**, *280*, 119453. [CrossRef]

26. Gao, J.; Song, J.; Ye, J.; Duan, X.; Dionsion, D.D.; Yadav, J.S.; Nadagouda, M.N.; Yang, L.; Luo, S. Comparative toxicity reduction potential of UV/sodium percarbonate and UV/hydrogen peroxide treatments for bisphenol A in water: An integrated analysis using chemical, computational, biological, and metabolomic approaches. *Water Res.* **2021**, *190*, 116755. [CrossRef]

27. Miao, Z.; Gu, X.; Lu, S.; Brusseau, M.L.; Zhang, X.; Fu, X.; Danish, M.; Qiu, Z.; Sui, Q. Enhancement effects of chelating agents on the degradation of tetrachloroethene in Fe(III) catalyzed percarbonate system. *Chem. Eng. J.* **2015**, *281*, 286–294. [CrossRef]

28. Sablas, M.M.; Luna, M.D.; Garcia-Segura, S.; Chen, C.W.; Dong, C.D. Percarbonate mediated advanced oxidation completely degrades recalcitrant pesticide imidacloprid: Role of reactive oxygen species and transformation products. *Sep. Purif. Technol.* **2020**, *250*, 117269. [CrossRef]

29. Tang, S.; Yuan, D.; Rao, Y.; Li, M.; Shi, G.; Gu, J.; Zhang, T. Percarbonate promoted antibiotic decomposition in dielectric barrier discharge plasma. *J. Hazard. Mater.* **2019**, *366*, 669–676. [CrossRef]

30. Wang, T.; Jia, H.; Guo, X.; Xia, T.; Qu, G.; Sun, Q.; Yin, X. Evaluation of the potential of dimethyl phthalate degradation in aqueous using sodium percarbonate activated by discharge plasma. *Chem. Eng. J.* **2018**, *346*, 65–76. [CrossRef]

31. Wei, C.; Zhang, F.; Yun, H.; Feng, C.; Wu, H. Ozonation in water treatment: The generation, basic properties of ozone and its practical application. *Rev. Chem. Eng.* **2016**, *33*, 49–89. [CrossRef]

32. Chen, H.L.; Lee, H.M.; Chen, S.H. Review of packed-bed plasma reactor for ozone generation and air pollution control. *Ind. Eng. Chem. Res.* **2008**, *47*, 2122–2130. [CrossRef]

33. Siraj, Z.; Maafa, I.M.; Shafig, I.; Shezad, N.; Akhter, P.; Yang, W.; Hussain, M. KIT-6 induced mesostructured TiO_2 for photocatalytic degradation of methyl blue. *Environ. Sci. Pollut. Res.* **2021**, *28*, 53340–53352. [CrossRef]

34. Tang, S.; Yuan, D.; Rao, Y.; Qi, J.; Cheng, T.; Sun, Z.; Gu, J.; Huang, H. Persulfate activation in gas phase surface discharge plasma for synergetic removal of antibiotic in water. *Chem. Eng. J.* **2018**, *337*, 446–454. [CrossRef]

35. Paździor, K.; Wrębiak, J.; Klepacz-Smółka, A.; Gmurek, M.; Bilińska, L.; Kos, L.; Sójka-Ledakowicz, J.; Ledakowicz, S. Influence of ozonation and biodegradation on toxicity of industrial textile wastewater. *J. Environ. Manag.* **2017**, *195*, 166–173. [CrossRef]

36. Fischbacher, A.; Sonntag, J.V.; Sonntag, C.V.; Schmidt, T.C. The ·OH radical yield in the H_2O_2 + O_3 (peroxone) reaction. *Environ. Sci. Technol.* **2013**, *47*, 9959–9964. [CrossRef]

37. Shang, K.; Wang, X.; Li, J.; Wang, H.; Lu, N.; Jiang, N.; Wu, Y. Synergetic degradation of acid orange 7 (AO7) dye by DBD plasma and persulfate. *Chem. Eng. J.* **2017**, *311*, 378–384. [CrossRef]

38. Kan, H.; Wang, T.; Yang, Z.; Wu, R.; Shen, J.; Qu, G.; Jia, H. High frequency discharge plasma induced plasticizer elimination in water: Removal performance and residual toxicity. *J. Hazard. Mater.* **2020**, *383*, 121185. [CrossRef]

39. Malik, M.A.; Ghaffar, A.; Malik, S.A. Water purification by electrical discharges. *Plasma Sources Sci. Technol.* **2001**, *10*, 82–91. [CrossRef]

40. Zhou, L.; Song, W.; Chen, Z.Q.; Yin, G.C. Degradation of organic pollutants in wastewater by bicarbonate activated hydrogen peroxide with supported cobalt catalyst. *Environ. Sci. Technol.* **2013**, *47*, 3833–3839. [CrossRef]

41. Wang, J.; Wang, K.; Zhang, Y.; Guo, L.; Guo, Z.; Sun, W.; Ye, Z.; Niu, J. Mechanism of bicarbonate enhancing the photodegradation of β-blockers in natural waters. *Water Res.* **2021**, *197*, 117078. [CrossRef] [PubMed]

42. Chen, W.; Westerhoff, P.; Leenheer, J.A.; Booksh, K. Fluorescence excitation-emission matrix regional integration to quantify spectra for dissolved organic matter. *Environ. Sci. Technol.* **2015**, *37*, 5701–5710. [CrossRef] [PubMed]

43. Zhu, G.; Fang, H.; Xiao, Y.; Hursthouse, A.S. The application of fluorescence spectroscopy for the investigation of dye degradation by chemical oxidation. *J. Fluoresc.* **2020**, *30*, 1271–1279. [CrossRef] [PubMed]

44. Guo, H.; Jiang, N.; Wang, H.; Shang, K.; Lu, N.; Li, J.; Wu, Y. Enhanced catalytic performance of graphene-TiO_2 nanocomposites for synergetic degradation of fluoroquinolone antibiotic in pulsed discharge plasma system. *Appl. Catal. B* **2019**, *248*, 552–566. [CrossRef]

45. He, Z.; Que, W.; Yin, X.; He, Y. Hydrogen titanium oxide hydrate: Excellent performance on degradation of methyl blue in aqueous solutions. *RSC Adv.* **2014**, *4*, 39678–39683. [CrossRef]

46. Zhang, T.; Oyama, T.; Aoshima, A.; Hidaka, H.; Zhao, J.; Serpone, N. Photooxidative N-demethylation of methylene blue in aqueous TiO_2 dispersions under UV Irradiation. *J. Photochem. Photobiol. A* **2001**, *140*, 163–172. [CrossRef]

47. Guo, H.; Wang, Y.; Yao, X.; Zhang, Y.; Li, Z.; Pan, S.; Han, J.; Xu, L.; Qiao, W.; Li, J.; et al. A comprehensive insight into plasma-catalytic removal of antibiotic oxytetracycline based on graphene-TiO_2-Fe_3O_4 nanocomposites. *Chem. Eng. J.* **2021**, *425*, 130614. [CrossRef]

48. Wang, Y.; Huang, J.; Guo, H.; Puyang, C.; Han, J.; Li, Y.; Ruan, Y. Mechanism and process of sulfamethoxazole decomposition with persulfate activated by pulse dielectric barrier discharge plasma. *Sep. Purif. Technol.* **2022**, *287*, 120540. [CrossRef]

49. Wang, X.; Wang, P.; Liu, X.; Hu, L.; Wang, Q.; Xu, P.; Zhang, G. Enhanced degradation of PFOA in water by dielectric barrier discharge plasma in a coaxial cylindrical structure with the assistance of peroxymonosulfate. *Chem. Eng. J.* **2020**, *389*, 124381. [CrossRef]

50. Guo, H.; Li, Z.; Xiang, L.; Jiang, N.; Zhang, Y.; Wang, H.; Li, J. Efficient removal of antibiotic thiamphenicol by pulsed discharge plasma coupled with complex catalysis using graphene-WO$_3$-Fe$_3$O$_4$ nanocomposites. *J. Hazard. Mater.* **2020**, *403*, 123673. [CrossRef]

51. Guo, H.; Yang, H.; Huang, J.; Tong, J.; Liu, X.; Wang, Y.; Qiao, W.; Han, J. Theoretical and experimental insight into plasma-catalytic degradation of aqueous p-nitrophenol with graphene-ZnO nanoparticles. *Sep. Purif. Technol.* **2022**, *295*, 121362. [CrossRef]

52. USEPA. *Toxicity Estimation Software Tool, Version 4.2.1*; U.S. Environmental Protection Agency: Washington, DC, USA, 2017.